Mixed *ab initio* quantum mechanical and Monte Carlo calculations of secondary emission from SiO_2 nanoclusters

Simone Taioli,[1,2] Stefano Simonucci,[3] Lucia Calliari,[1] Massimiliano Filippi,[1] and Maurizio Dapor[1,2]
[1]*FBK-IRST Center for Materials and Microsystems, Via Sommarive 18, 38050 Povo (Trento), Italy*
[2]*The European Centre for Theoretical Studies in Nuclear Physics and Related Areas, Strada delle Tabarelle 286, I-38050 Villazzano (Trento), Italy*
[3]*Department of Physics, University of Camerino, via Madonna delle Carceri 9, 62032 Camerino, Italy*
(Received 19 November 2008; revised manuscript received 20 January 2009; published 27 February 2009)

A mixed quantum mechanical and Monte Carlo method for calculating Auger spectra from nanoclusters is presented. The approach, based on a cluster method, consists of two steps. *Ab initio* quantum mechanical calculations are first performed to obtain accurate energy and probability distributions of the generated Auger electrons. In a second step, using the calculated line shape as electron source, the Monte Carlo method is used to simulate the effect of inelastic losses on the original Auger line shape. The resulting spectrum can be directly compared to "as-acquired" experimental spectra, thus avoiding background subtraction or deconvolution procedures. As a case study, the O *K-LL* spectrum from solid SiO_2 is considered. Spectra computed before or after the electron has traveled through the solid, i.e., unaffected or affected by extrinsic energy losses, are compared to the pertinent experimental spectra measured within our group. Both transition energies and relative intensities are well reproduced.

DOI: 10.1103/PhysRevB.79.085432 PACS number(s): 71.15.−m, 03.65.Nk, 02.70.Uu, 78.70.−g

I. INTRODUCTION

In recent years, remarkable developments in two branches of semiconductor physics have been achieved. One is the theoretical advance in the study of band gaps and quasiparticle spectra in systems, notably transition-metal oxides, where electronic correlation creates states other than simple Fermi gas.[1] The other is the science of nanomaterials whose electronic, spectroscopic, and transport properties bridge the gap between molecules and condensed matter.[2] The search for new technologies in nanoelectronics based on silicon and carbon nanomaterials[3,4] has been fueled by the potential applications of such nanoclusters as junctions in optical telecommunication networks or in integrated circuits where serious obstacles are represented by both the signal speed and spatial density. Despite many recent advances in the development of carbon-based electronics,[5] silicon still represents the most widely used physical means. Furthermore, a miniaturization of silicon-based devices would retain all our understanding of the physics of this semiconductor and the technological background of the microelectronics industry. But while the knowledge of the electronic properties of silicon and silicon oxides has advanced greatly, largely due to the development of theories capable of treating the correlation energy,[6] theoretical results on the secondary emission and energy loss mechanisms are still the subject of discussion.[7]

In this paper, we focus on the O *K-LL* spectrum from SiO_2 clusters. We present a combination of an *ab initio* quantum mechanical (QM) method with Monte Carlo simulations (QMMC) to calculate nonradiative decay spectra from SiO_2 nanoclusters of different sizes taking into account postcollisional interactions (PCIs) due to electron dynamical screening. The method is validated by comparison to measured spectra obtained by our group. In this regard, we move along two independent directions. On one hand, we start from the measured spectrum, affected by all kinds of energy losses suffered by the electron on its way out of the solid, and we recover the "true" Auger spectrum by conventional deconvolution procedures. On the other hand, using the computed O *K-LL* spectrum as electron source, we use the Monte Carlo method to simulate the effect of inelastic scattering on the original electron energy distribution. A key ingredient for both procedures is the inelastic-scattering cross section or, equivalently, the reflection electron energy loss spectrum (REELS). While the well studied[8–10] O *K-LL* spectrum from SiO_2 clusters is taken here as a case study, we believe that our approach is sufficiently general to be applied to the interpretation of core electron spectroscopies, such as photoemission (PES), Auger (AES), and autoionization by taking into account dynamical screening effects in a variety of nanoclusters and condensed-matter systems.

In order to gain new insights into the nature of correlation and of continuum states in nanoclusters, a number of well-defined questions have to be addressed. What is the nature of the fundamental process occurring in a scattering experiment, where an electron or a photon is injected in the topmost layer? What is the nature of the core-hole and double-hole states when electronic relaxations and charge disorder are included? How does hole localization distort the double-hole density of states (DOS) and manifest itself in the scattering process? What is the role of dynamical screening in the Auger process? Can the above considerations be combined to understand experimental data in a unified framework? Are the results size dependent?

Many models, described in several reviews,[11–14] have been suggested to tackle the calculation of Auger spectra in solids, a difficult task due to the high number of energy levels involved and the contribution of additional degrees of freedom which broaden line shapes. In particular, computational and theoretical procedures are represented by methods developed by Tarantelli and Cederbaum,[15] Averbukh and

Cederbaum,[16] Ohno and Wendin,[17] and Verdozzi *et al.*[18] In each of these cases, Auger decay probabilities were computed by means of atomic Auger matrix elements with the many-body Green's function projected onto atomic states and the spectral line shape obtained by calculating the residua of such a projected quantity. This approach revealed very valuable in the calculation of atomic and molecular[19–21] Auger spectra, but the extension to solids is fairly difficult and poor in results. Verdozzi *et al.*[18,22] improved such an approach to separate the atomic features from those characteristic of a periodic structure (see below). The striking difference between our approach and those used by all the above cited authors (and further extensions of their work) lies in the computation of the many-body Green's function. In fact, in our method the many-body Green's function is projected onto "localized" states, which are a "local mixture" of atomic states. Therefore, differently from previous works, our local projectors are multicentered and may include some atomic space points. In other words, the role played by our projectors is somehow similar to that played by localized Wannier functions in solid-state calculations. It is clear that the use of localized (not atomic) Auger matrix elements will prove to be very valuable in the treatment of transitions, such as valence-valence-valence (V-VV), where initial states are not atomic, but delocalized in nature. The quest of multicenter projectors in the calculation of Auger matrix elements is of paramount importance because the use of atomic Auger matrix elements, acceptable in molecular spectra, would result in a crude approximation for condensed-matter core-hole spectroscopy.

As for core-valence-valence (C-VV) spectra, their understanding is presently based on the use of atomic transition matrix elements and it is rooted in Lander's original idea[23] that such spectra should basically reflect the self-convolution of the valence-band DOS, the so-called "bandlike" spectra. While this is true for solids such as Li and Si, it fails for transition metals, Zn for example, whose C-VV spectra are instead referred to as "atomiclike." Recognizing that correlation effects between the two final-state holes were responsible for such spectra led to the Cini-Sawatzky theory[24,25] which, derived at first only for systems with initially filled bands, has since become the framework for any quantitative interpretation of C-VV spectra. Within this model, hole-hole correlation energy is a semiempirical parameter to be determined by comparison with measured spectra. In particular, the effect of hole-hole repulsion on the O *K-LL* spectrum from bulk SiO_2 has been recently investigated by van Riessen *et al.*[8] using the Cini-Sawatzky model extended by Ramaker.[9] The spectrum is computed by multiplying experimental intra-atomic transition matrix elements by the distorted DOS due to hole localization. Despite O *K-LL* spectrum could be satisfactorily reproduced, matrix elements and characteristic parameters were taken from atoms, a fact that can be inappropriate for ionic crystals, such as SiO_2, where occupation numbers are different from the atomic ones.

The calculation presented here represents an attempt to address the questions listed above from first principles, with a full *ab initio* treatment of hole-hole correlation and taking into account collective excitations without free parameters, except for a constant factor to normalize spectral intensity. We will focus on the so-called principal or normal Auger process, whereas the contribution of satellites (associated with shake processes) to the Auger spectrum is neglected.

II. THEORY

The general theoretical framework for interpreting Auger decay in nanoclusters is the theory of scattering,[26] where the initial state consists of a projectile, in our case typically photons or electrons, and a target in its ground state, while the final states are characterized by an ionized system and one or more electrons asymptotically noninteracting. The main problem to be addressed for the calculation of the Auger theoretical spectrum is the construction of a continuum electronic wave function that accurately takes into account correlation effects among electrons bound in the nanoclusters and between the escaping and bound electrons. To build this wave function we need to extend a method[27,28] that already successfully applied to the calculation of inner-shell spectra in small molecules, such as CO (Ref. 29) and C_2H_2.[30,31] However, the existence of several interacting decay paths, quantum effects due to complex many-body interactions and localization/delocalization effects, make such extension very difficult if one wants to keep the computational cost comparable to that of molecules.

To compute the scattering wave functions $|\Psi^-_{\alpha,\varepsilon_\alpha}\rangle$, including the appropriate *incoming wave* boundary conditions, we use an approach based on Fano's multichannel theory,[32] where the solution to the scattering process is represented by a linear combination of a metastable state $|\Phi\rangle$ with states embedded in the noninteracting continuum many-fold $\{\chi^-_{\beta,\varepsilon_\beta}\}$,

$$|\Psi^-_{\alpha,\mathcal{E}}\rangle = |\chi^-_{\alpha,\varepsilon_\alpha}\rangle + \frac{M^-_\alpha(\varepsilon_\alpha,E)}{E-E_r-i\frac{\Gamma}{2}} \times \left[|\Phi\rangle + \lim_{\nu\to 0}\sum_\beta \int_0^\infty \frac{|\chi^-_{\beta,\tau}\rangle M^-_\beta(\tau,E)^*}{E-E_\beta-\tau-i\nu}d\tau\right] \quad (1)$$

with Γ and $M^-_\beta(\varepsilon_\beta,E)$ defined as follows:

$$\Gamma = \sum_\beta \Gamma_\beta = 2\pi\sum_\beta |M^-_\beta(\varepsilon_\beta,E)|^2, \quad (2)$$

$$M^-_\beta(\varepsilon_\beta,E) = \langle\Phi|H-E|\chi^-_{\beta,\varepsilon}\rangle, \quad \varepsilon_\beta = E_r - E_\beta. \quad (3)$$

In Eqs. (1)–(3) E_r is the energy of the resonant state modified by the interaction with the continuum states $\{\chi^-_{\beta,\varepsilon_\beta}\}$ and E_β is the energy of final states. These multichannel continuum wave functions can be obtained from a set of interacting continuum states $\{\chi_{\beta,\varepsilon_\beta}\}$, coupled by the interchannel interaction, by projecting the Hamiltonian H on a finite set of multicentered L^2 functions spanning the Hilbert space in the range of the ejected electron kinetic energy,

$$\langle\chi_{\beta\varepsilon_\beta}|\hat{H}-E|\chi_{\alpha\varepsilon_\alpha}\rangle = \langle\psi_{\varepsilon_\beta};\beta|\hat{\mathcal{H}}(E)-E|\psi_{\varepsilon_\alpha};\alpha\rangle, \quad (4)$$

where $|\psi_{\varepsilon_\beta};\beta\rangle$ represents the antisymmetric tensorial product of the escaping electron wave function at energy ε_β with the

doubly ionized target wave function (β). In Eq. (4) $\hat{\mathcal{H}}$ is the projected Hamiltonian, which includes the projected scattering potential

$$\hat{V}^{\beta,\alpha}(\varepsilon_\beta,\varepsilon_\alpha) = \langle \chi_{\beta\varepsilon_\beta} | \hat{V} | \chi_{\alpha\varepsilon_\alpha} \rangle \tag{5}$$

describing the interchannel interaction among bound and emitted electrons in the scattering region.

To find an accurate solution of Eq. (4) in SiO_2 nanoclusters, a number of numerical and theoretical techniques have been implemented. The first problem is the choice of the basis set for the bound states and the scattering wave function. Due to the large number of atoms and open channels in comparison to molecules, the size of the Hilbert space where the wave functions are expanded increases rapidly for nanoclusters. An increasing number of Gaussians may lead to convergence to nonphysical states due to basis set superposition errors and linear dependence problems,[33] particularly in the calculation of metastable states. In order to keep the number of excited determinants in the doubly ionized target low, we split the problem in two steps: we first calculate the bound orbitals in a restricted Gaussian basis set; we then include an auxiliary basis set of modified Gaussian functions to compute the matrix elements of the scattering potential [Eq. (5)]. The Hartree-Fock procedure takes the variationally optimized atomic wave functions of different components of the nanocluster as a starting point for the calculation of the nanocluster wave functions, ensuring the convergence of the multiconfiguration procedure[34] to the appropriate ionic states within the space spanned by a minimal basis set. An adequate representation of the continuum orbital, comparable to the solution of the multiconfiguration procedure in bound orbitals, forces us to enlarge the basis set in scattering-wave-function calculations. We emphasize that the scattering basis set is built with a diffuse Gaussian basis set multiplied by symmetry-adapted Hermite polynomials to reproduce the oscillating behavior of the continuum wave functions inside the scattering region. This enlarged basis set is used both in the expansion of the continuum orbital and in the projection of the interchannel coupling inside the Hilbert space spanned by the interacting decay channels. Continuum orbitals have to be orthogonal to bound orbitals. To satisfy this constraint one can use two different methodologies. One is direct orthogonalization and the other uses projection of the kinetic operator onto the orthogonal complement of the bound states. The latter procedure defines an effective potential, which has the same structure of the Phillips-Kleinman potential[35] used in condensed-matter calculations for building valence orbitals orthogonal to the core states. Surprisingly, we found that the Phillips-Kleinman technique leads to numerical instabilities, with a basis set dependence, in the calculation of the SiO_2 nanoclusters continuum density of states. It turned out that such instability is found whenever the eigenvalues of the metrics of the chosen basis set are smaller than 10^{-4}. Attention has to be paid, when choosing the basis set, to describe appropriately the scattering potential in the energy region where electrons are emitted and to avoid a small overlap between the basis elements. After taking into account such a criterion, calculations of the continuum density of states for SiO_2 nanoclusters gave the same results in terms of either approach used to satisfy the orthogonality constraint.

Due to the enormous number of decay channels coupled with the final states, the Auger probability in nanocluster calculations is spread all over the bands with a complex distribution. Accordingly, the computational cost to evaluate the interchannel potential in Eq. (5), responsible for the interaction between the open channels and for the probability spread among the noninteracting channels, may be so high that it could not be directly performed as previously done for molecules.[36] Unfortunately, interchannel interaction cannot be neglected because its absence is the main source of errors and of large discrepancies with experimental spectra in scattering calculations.[36]

One can argue that the strong ionic bond between Si and O leads to a rather large interaction. The electronic cloud distortion, with silicon to oxygen charge donation, favors holes trapping on the oxygen site. Moreover, small multisite interaction among the SiO_2 units is responsible for the narrow valence bandwidth. As a consequence, one expects a very low hole mobility, clamped down by a large hole-hole interaction. From these observations, one expects that the final states are created by intra-atomic transitions with the two holes strongly localized.

In light of what we have shown above, a theoretical approach for calculating atomiclike and bandlike Auger line shapes in nanoclusters with strong correlation effects is proposed here. In this method both the initial-state core-hole and the final-state valence holes are first localized on the central atom and multisite interactions enter naturally in the model Hamiltonian as a perturbation. Therefore, a number of localized states, which account for the majority of the decay probability, are selected among the open channels. These "tight-binding" states are further coupled via the interchannel potential in such a way that the model Hamiltonian can be diagonalized at a very high level of accuracy in a smaller space, corresponding to the most intense open channels. This calculation results in a number of noninteracting states, which account for the quasiatomic behavior of the nanocluster. The long-range or bandlike behavior of the Auger decay is calculated at this stage by switching on the weak multisite interaction. The perturbative coupling of each noninteracting channel with a number of states describing transitions close in energy, allows us to choose, among the degenerate states, those presenting a maximum overlap with the selected channel and, therefore, to obtain the whole line shape.

III. CASE STUDY: SiO_2

To test our approach, we take the $Si_2O_7H_6$ nanocluster as representative of bulk SiO_2 to calculate the normal O *K-LL* Auger spectrum. Within the Born-Oppenheimer approximation, the optimized structure of $Si_2O_7H_6$ with a central oxygen atom has been obtained by minimizing the free energy of the electrons at each nuclei position with a smooth Fermi-Dirac smearing, relaxing the atomic bond length until the forces are less than 0.01 eV/Å per atom. The resulting atomic configuration is plotted in Fig. 1. Stars of neighbors,

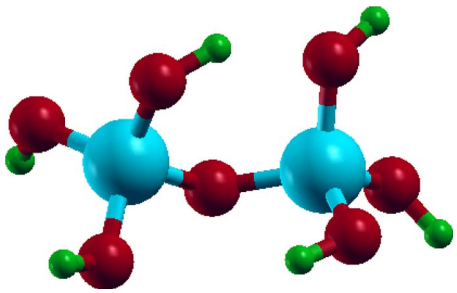

FIG. 1. (Color online) Sketch of the SiO_2 nanocluster optimized structure. Oxygen atoms are in red (dark gray), silicon atoms are in light blue (light gray), and hydrogen atoms are in green (smallest medium gray).

centered on the central oxygen atom, are found at a distance of $3.103a_0$ for silicon atoms and $4.953a_0$ for oxygen atoms. The present results are in good agreement with previous calculations on band structure and geometry of similar SiO_2 clusters.[37] Following our scheme, correlation in the initial state of the ionized target, characterized by a single inner vacancy in the $1s$ orbital of the central oxygen, and in the final states of the doubly ionized nanocluster, characterized by two vacancies in the valence orbitals, has been treated by extended configuration interaction (CI) expansion using the $3s,3p,3d$ orbitals of silicon and $3s,3p,3d$ of oxygen. Calculations of the bound states have been carried out using a basis set of Hermite Gaussian functions with (s,p,d)-type character centered on the nuclei. The basis set has been obtained by a variational procedure, optimizing the exponents of the standard 6–31 G^* basis set. In more detail we scan a finite range of values above and below the proposed 6–31 G^* ones, taking the values which lower the total energy. An auxiliary basis set, more dense and enlarged with diffuse functions, has been used to represent properly the projected potential $V^{\beta,\alpha}$ in Eq. (5), until variational stability of the Auger decay rate with respect to changes in the basis set is reached. This criterion allows an accurate description of the continuum orbitals around the Auger decay energies. The scattering calculations highlight the fundamental role of d-symmetry functions in the expansion of the projected potential. The resulting basis set is made up of $[9s(=4s_{Si}+3s_O+2s_H)+6p(=3p_{Si}+2p_O+1p_H)+3d(=1d_{Si}+2d_O)]$ contracted Hermite Gaussian functions for a total of 215 contracted Gaussians. The exponents $\alpha_s,\alpha_p,\alpha_d$ are in the ranges $[\alpha_s^{Si}=0.001-1.0,\alpha_p^{Si}=0.004-1.2,\alpha_d^{Si}=1.0]$ for the (s,p,d)-type Gaussians on silicon atoms, $[\alpha_s^{O}=0.002-0.5,\alpha_p^{O}=0.07-1.0,\alpha_d^{O}=1.0]$ for the (s,p,d)-type Gaussians on oxygen atoms, and $[\alpha_s^{H}=0.03-1.0,\alpha_p^{H}=1.0]$ for the (s,p)-type Gaussians on hydrogen atoms. We adopted a larger basis set on the central oxygen with $[4s+4p+3d]$ to properly represent hole localization effects. The examined nanocluster has an ionic character, with the central oxygen atom in the Si_2O unit found in the $Si^{+1.49}O^{-1.20}$ charge configuration. We found that the $Si_2O_7H_6$ nanocluster correctly reproduces one electron properties, localization effects, and the charge population of solid SiO_2. In Table I we have reported the energies, referred to the vacuum level, and the relative decay rates of the most intense 15 transitions, all with double holes localized on the central oxygen atom, obtained after switching on the interchannel coupling.

IV. EXPERIMENTAL DATA HANDLING

Since first-principles methods necessarily involve approximations, the most important of which, in scattering calculations, is the approximate form of the electron wave function in the continuum, it is important to validate the calculations against experimental data. To this end, O *K-LL* spectra were measured from a 36-nm-thick SiO_2 film grown on a Si substrate. The film surface was cleaned by annealing at 800 °C in a ultrahigh vacuum preparation chamber connected to the analysis chamber (base pressure 2×10^{-10} mbar). The analysis chamber is a PHI545 instrument equipped with double-pass cylindrical mirror analyzer, coaxial electron gun, nonmonochromatic Mg $K\alpha$ x-ray source, and He discharge lamp. The x-ray ($h\nu=1253.6$ eV) excited O *K-LL* spectrum was recorded at constant analyzer energy resolution, $\Delta E=0.6$ eV, as measured on the Pd Fermi edge of a HeI ($h\nu=21.2$ eV) excited valence-band photoemission spectrum. A reflection electron energy loss spectrum, excited from the same sample by 500 eV electrons, i.e., near the kinetic energy of O *K-LL* electrons, was acquired within the same instrument and at the same analyzer resolution of the Auger spectrum. To keep electron-beam-induced damage to a minimum, the current density was

TABLE I. Kinetic energies (E_{kin}) in eV, referred to the vacuum level, and probabilities (Γ_α) in arbitrary units for the O *K-LL* Auger localized states of $Si_2O_7H_6$ nanocluster according to the double-hole configurations (O *K-LL*) in the central oxygen atom and final total spin S^2 (0=singlet, 1=triplet).

O *K-LL*	S^2	E_{kin}	Γ_α	O *K-LL*	S^2	E_{kin}	Γ_α
2*s*-2*s*	(0)	458.75	0.281	2*p*-2*p*	(0)	497.89	0.395
2*s*-2*p*	(0)	473.4	0.252	2*p*-2*p*	(0)	498.74	0.425
2*s*-2*p*	(0)	477.41	0.322	2*p*-2*p*	(1)	499.88	0.003
2*s*-2*p*	(0)	477.99	0.308	2*p*-2*p*	(0)	500.28	0.409
2*s*-2*p*	(1)	481.64	0.077	2*p*-2*p*	(0)	501.98	0.481
2*s*-2*p*	(1)	484.96	0.090	2*p*-2*p*	(0)	502.45	0.493
2*s*-2*p*	(1)	485.73	0.094	2*p*-2*p*	(1)	504.13	0.003
2*p*-2*p*	(0)	493.94	0.330				

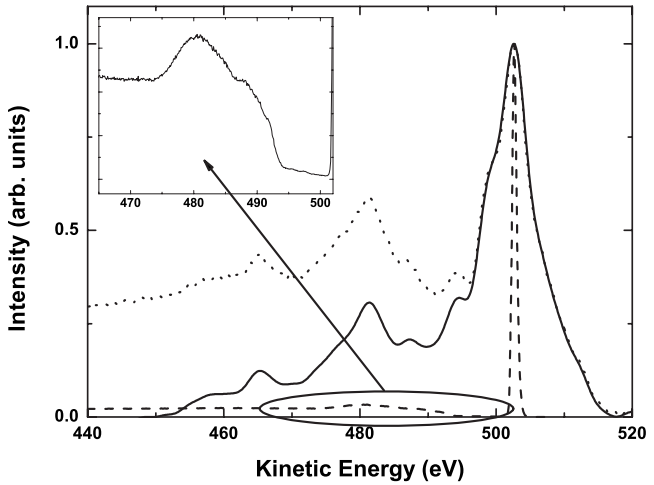

FIG. 2. Plot of the experimental data. The x-ray ($h\nu$ =1253.6 eV) excited O *K-LL* spectrum (continuous line) has been obtained by deconvolution of a REEL spectrum (dashed line) from a spectrum obtained by subtracting a constant background, defined by the region immediately to the right (520–530 eV) of the main peak (dotted line).

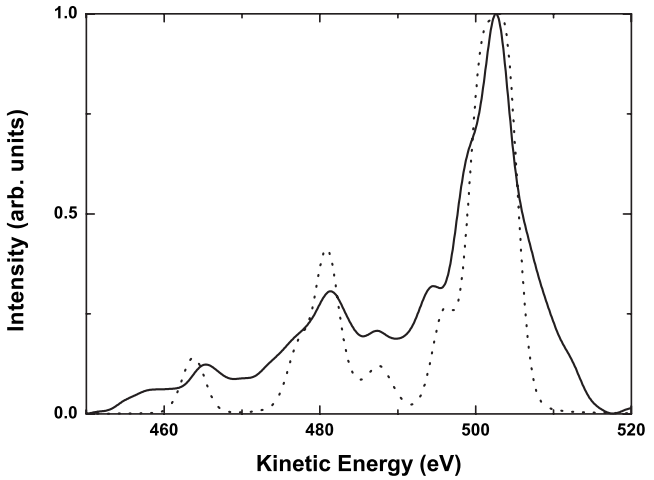

FIG. 3. O *K-LL* Auger spectrum in $Si_2O_7H_6$. Comparison between the QM theoretical data (dotted line) and the experimental data after deconvolution of a REEL spectrum (continuous line).

lower than 40 A/m^2 and the acquisition time was lower than 6 min. The energy scale was calibrated on clean Au and Cu, following recommended procedures.[38] Kinetic energies are referred to the vacuum level.

As-acquired spectra were corrected for the energy dependence of the analyzer transmission function. The latter had been previously determined on clean Au, Ag, and Cu as explained in Ref. 39. A constant background, defined by the region immediately to the right (520–530 eV) of the main peak in the O *K-LL* spectrum, was subtracted and the intensity was normalized to unit height of the main peak, resulting in the spectrum (dotted line) shown in Fig. 2. Also plotted in Fig. 2 is the REEL spectrum (dashed line) which includes the so-called elastic or zero loss peak together with the associated inelastic losses. The spectrum is slightly shifted in energy, so that the zero loss peak is aligned to the main O *K-LL* peak. Its intensity is normalized to unit height of the zero loss peak. A vertical expansion of the loss features is shown in the inset. By deconvoluting the REEL spectrum from the measured O *K-LL* spectrum, the O *K-LL* line shape given by the continuous line in Fig. 2 was finally obtained.

V. LINE-SHAPE ANALYSIS

This spectrum is compared to the *ab initio* calculated O *K-LL* spectrum in Fig. 3. The computed spectrum is generated by convoluting the theoretical transition rates with a Voigt profile to take into account both the bandwidth of the x-ray source and the finite resolving power of the electron spectrometer. This results in a convolution of a Gaussian with Σ_g=1 eV, according to our instrument resolution, and a Lorentzian with Σ_l=0.1 eV, which is the computed total Auger decay rate. Both spectra are normalized to a common height of the main peak, while no energy shift was required to obtain the kind of agreement shown in the figure. We observe that our calculation correctly reproduces transition energies. These are distributed over three different regions. From right to left, features between 494 and 510 eV are due to $2p$-$2p$ hole configurations in the final states (K-$L_{23}L_{23}$ transitions); the most intense peaks are singlet transitions around [501–503] eV (maximum at 502.76 eV), close to the experimental peak (502.58 eV). Between 475 and 492 eV a second group of features is found, where the hole configuration in the final states is $2s$-$2p$ (K-L_1L_{23} transitions); the most intense peaks are singlet transitions around [480–482] eV (maximum at 481.1 eV), close to the experimental peak (481.38 eV). Finally a third group of features is observed between 460 and 470 eV, where the hole configuration in the final states is $2s$-$2s$ (K-L_1L_1 transitions); the most intense peaks are singlet transitions around [463–465] eV (maximum at 463.86 eV), lower than the experimental peak (465.25 eV). In general the most intense peaks are singlet transitions with both holes on the central oxygen atom, whereas the shoulders are triplet transitions, unfavored by selection rules.

Besides transition energies, also calculated values of the decay rates are satisfactorily reproduced in Fig. 3, meaning that the adopted scattering basis set is appropriate to represent the projected potential within the scattering region for any channel. However, the *ss* and *sp* contributions are slightly overestimated. This is due to lack of electronic correlation or to dynamic screening effects[14] in the CI calculation. The size of the excited determinants space in the CI procedure for both the intermediate core-hole and double ionized final states has been chosen large enough to reproduce well transition energies and decay probabilities, but a larger active space should be, in principle, adopted to take into account hole delocalization on all valence bands and electronic excitations. Furthermore, the localized (not atomic) Auger matrix elements are kept fixed during this procedure and their square modulus enters as a multiplicative factor in the line-shape analysis. In principle, they should be updated with a new electronic continuum wave function derived by a multichannel procedure, taking into account the

correlation between the double ion and the new escaping electron wave function. Larger CI calculations, although computationally very expensive, would correct the line shape for the overestimation of the s to p contribution. The same kind of agreement seen in Fig. 3 is obtained by comparing our calculated O *K-LL* Auger spectrum to the measured spectrum by van Riessen *et al.*[8] and Ramaker *et al.*[10] Without loss of accuracy the present method thus allows us to calculate the Auger line shape in nanostructures and solids at a computational cost comparable to that typical for atoms and molecules.

VI. MONTE CARLO SCHEME: QMMC VERSUS MEASURED SPECTRUM

As stated above, the comparison between computed and experimental spectra requires accounting for changes caused to the original electron energy distribution by energy losses suffered by the Auger electron on its way out of the solid. The typical procedure in this respect is the one described above. Alternatively however, one could simulate the effects of inelastic losses on the "original" distribution. The basic idea is to use the *ab initio* Auger probability distribution as a source of electrons which undergo inelastic processes. Within our model the *ab initio* spectrum could include the intrinsic energy loss due to shake processes. As stated above, however, shake processes were neglected in the present paper. On the other hand, extrinsic energy losses, due to the interaction with collective degrees of freedom of the valence charge (valence plasmons[40]) and to multiple inelastic scatterings, should be dealt with after computing the spectrum and using statistical methods. In this way inelastic background would be superimposed to the theoretical spectrum instead of removing it, a procedure not free from uncertainty. Possible effects of background subtraction on the spectrum final shape are discussed, for example, in Ref. 41.

The simplest approach to account for the extrinsic loss is the Monte Carlo method.[42] Details of the Monte Carlo scheme describing electron energy losses in silicon dioxide were given in previous works.[43–45] In the following we will briefly summarize the numerical approach used in this paper. The theoretical Auger spectrum previously calculated is assumed to be the initial energy distribution of the escaping electrons. The stochastic process for multiple scattering follows a Poisson-type law. The step length Δs is given by $\Delta s = -\lambda \ln(\mu_1)$, where μ_1 is a random number uniformly distributed in the range $[0,1]$. λ is the electron mean-free path,

$$\lambda(E) = \frac{1}{N[\sigma_{\mathrm{el}}(E) + \sigma_{\mathrm{inel}}(E)]}, \tag{6}$$

where N is the number of SiO_2 molecules per unit volume, $\sigma_{\mathrm{el}}(E)$ is total elastic-scattering cross section, and $\sigma_{\mathrm{inel}}(E)$ is the total inelastic-scattering cross section at the impinging electron kinetic energy E. The calculation of differential and total elastic-scattering cross sections was performed by the relativistic partial wave expansion method,[43,46,47] whereas differential and total inelastic-scattering cross sections were computed using the Ritchie theory.[48] Taking Buechner's experimental optical data[49] for the evaluation of the long-wavelength limit of the dielectric function $\varepsilon(\omega)$, one obtains the differential inelastic-scattering cross section as

$$\frac{d\sigma_{\mathrm{inel}}(E,\omega)}{d\omega} = \frac{me^2}{2\pi\hbar^2 NE}\mathrm{Im}\left[\frac{-1}{\varepsilon(\omega)}\right] S\left(\frac{\omega}{E}\right), \tag{7}$$

where ω is the energy loss and, according to Ashley,[50] the function S is given by

$$S(x) = (1-x)\ln\frac{4}{x} - \frac{7}{4}x + x^{3/2} - \frac{33}{32}x^2. \tag{8}$$

Before each collision, a random number μ_2 uniformly distributed in the range $[0,1]$ is generated and compared with the probability of inelastic scattering $q_{\mathrm{inel}} = \sigma_{\mathrm{inel}}/(\sigma_{\mathrm{inel}} + \sigma_{\mathrm{el}})$. When μ_2 is smaller or equal to the probability of inelastic scattering, then the collision is inelastic; otherwise, it is elastic. If the collision is elastic, θ, the polar scattering angle, is selected so that the integrated scattering probability in the range $[0,\theta]$ is equal to the random number μ_3 uniformly distributed in the range $[0,1]$,

$$\mu_3 = \frac{1}{\sigma_{\mathrm{el}}}\int_0^{\theta}\frac{d\sigma_{\mathrm{el}}}{d\Omega} 2\pi \sin\vartheta d\vartheta, \tag{9}$$

where Ω is the solid angle of scattering. If the collision is inelastic, the energy loss W of an incident electron with kinetic energy E is computed via a random number μ_4, uniformly distributed in the range $[0,1]$,

$$\mu_4 = \frac{1}{\sigma_{\mathrm{inel}}}\int_0^{W}\frac{d\sigma_{\mathrm{inel}}}{d\omega} d\omega, \tag{10}$$

Auger electron generation is simulated assuming a constant depth distribution whose thickness, according to Ref. 8, was set to 40 Å. To obtain good accuracy in the results the number of random walks is 10^8. A plot of the QMMC calculation compared to the experimental data before deconvolution of energy losses is given in Fig. 4. The original theoretical spectrum is also shown for reference. One can see that QMMC

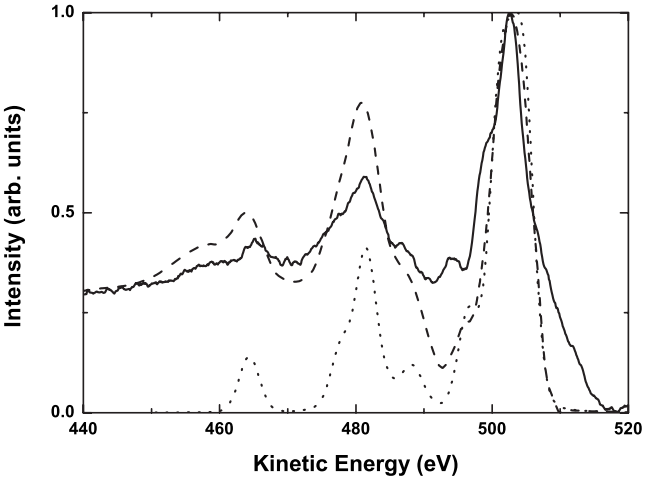

FIG. 4. O *K-LL* Auger spectrum in $Si_2O_7H_6$. Comparison between the quantum mechanical theoretical data (dotted line), the Monte Carlo results (dashed line), and the original experimental data (continuous line).

enhances and broadens the Auger probability increasingly upon decreasing the electron kinetic energy. The large broadening of the K-$L_1L_{2,3}$ peak after Monte Carlo treatment is due to the main plasmon of SiO_2 [see inset in Fig. 2], whose distance from the zero loss peak is the same as the distance between the K-$L_{23}L_{23}$ and K-L_1L_{23} features in the Auger spectrum.

VII. CLUSTER SIZE EFFECTS

Since we are dealing with nanoclusters, it makes sense to assess the dependence of correlation effects on the cluster size. It is well known that an increasing number of atoms in the cluster causes the one-electron DOS to approach the band DOS of the solid. Increasing the number of atoms to simulate a bulk situation enlarges the number of available transitions to the final states to a point where the computational cost is enormous, while no appreciable change in the spectroscopic observables is obtained. In fact, the quasiatomic nature of Auger emission found in our *ab initio* calculations forces the hole-hole DOS to be centered on the atom where the initial core-hole has been created. We have investigated the role of cluster size by carrying out calculations on a smaller cluster of atoms, Si_2OH_6, to see how it compares with the bigger cluster. This nanocluster represents the minimal cluster size which still describes the chemical environment found in solid SiO_2. In Fig. 5, we compare the calculated O K-LL spectrum of Si_2OH_6 (dotted line) to that of $Si_2O_7H_6$ (continuous line). The experimental spectrum is also superimposed (dashed line). All spectra are normalized to a common height of the main peak, while no energy shift is performed. The two computed spectra were obtained by convolution with the same Voigt profile. We see that the main features of the spectrum are already consistently reproduced in the smaller cluster, although with a shift toward high energies. This "chemical shift" decreases from 2.52 to 1.45 eV on moving from the low-energy to the high-energy peak. This is a predictable consequence of the fact that Si dangling bonds are saturated with different elements for the two clusters (H for the smaller cluster and O for the bigger one) with a nonlocal dependence which is larger for lower angular momenta. Moreover, we observe that the $Si_2O_7H_6$ line shape is less resolved than the corresponding Si_2OH_6 one, as expected due to the increased number of decay channels. Although the two computed spectra do not differ much in the number of features and in relative decay rates, the overall agreement with the experimental spectrum slightly favors the bigger cluster. This observation confirms that our cluster approach is well suited for the calculation of Auger line shapes from bulk materials and that the 15-atom cluster considered in the present paper is near to the optimal size. In conclusion, we believe that enlarging further the cluster would not change substantially the Auger spectral line shape as expected on the basis of the local nature of AES. Inclusion, in the computed spectrum, of shake-up and shake-off transitions and of interactions between crystal phonons and escaping electron would result in a broadening of the line shape, correcting for the difference between the computed and experimental linewidths.

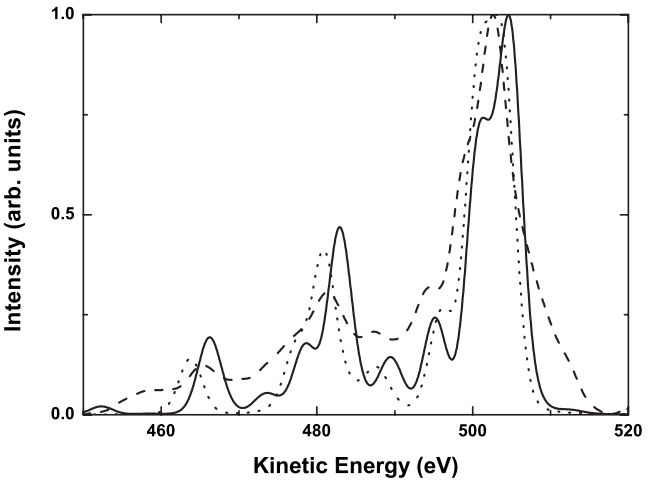

FIG. 5. Comparison between the O K-LL spectrum in Si_2OH_6 (dotted line), $Si_2O_7H_6$ (continuous line), and experimental data (dashed line).

VIII. CONCLUSIONS

We have demonstrated the potentiality of our first-principles model for calculating and predicting the line shapes of x-ray excited Auger electron spectra from silicon dioxide nanoclusters. Furthermore, a Monte Carlo analysis has been applied to the quantum mechanical computation of spectra to mimic the electron energy loss in condensed matter. Comparison to our experimental data reveals a satisfactory agreement, in the energy position and relative intensities of peaks and in the background contribution over the entire investigated energy range.

[1] L. Hedin, Phys. Rev. **139**, A796 (1965).
[2] C. Gerber and H. P. Lang, Nat. Nanotechnol. **1**, 3 (2006).
[3] Sang Soo Kim, Won-Ju Cho, Chang-Geun Ahn, Kiju Im, Jong-Heon Yang, In-Bok Baek, Seongjae Lee, and Koeng Su Lim, Appl. Phys. Lett. **88**, 223502 (2006).
[4] A. Jori, M. Dresses, and G. Dresses, *Topics in Applied Physics* (Springer, Berlin, 2008).
[5] P. Avouris, Z. Chen, and V. Probings, Nat. Nanotechnol. **2**, 605 (2007).
[6] F. Aryasetiawan and O. Gunnarsson, Rep. Prog. Phys. **61**, 237 (1998).
[7] W. S. M. Werner, *Slow Heavy Particle Induced Electron Emission from Solid Surfaces*, Springer Tracts in Modern Physics Vol. 225 (Springer, Berlin, 2007).
[8] G. A. van Riessen, S. M. Thurgate, and D. E. Ramaker, J. Electron Spectrosc. Relat. Phenom. **161**, 150 (2007).

[9] D. E. Ramaker, Phys. Rev. B **21**, 4608 (1980).
[10] D. E. Ramaker, J. S. Murday, N. H. Turner, G. Moore, M. G. Lagally, and J. Houston, Phys. Rev. B **19**, 5375 (1979).
[11] R. Weissmann and K. Müller, Surf. Sci. Rep. **1**, 251 (1981).
[12] P. Weightman, Rep. Prog. Phys. **45**, 753 (1982).
[13] G. G. Kleiman, Appl. Surf. Sci. **11-12**, 730 (1982).
[14] D. E. Ramaker, Crit. Rev. Solid State Mater. Sci. **17**, 211 (1991).
[15] F. L. S. Tarantelli, L. S. Cederbaum, A. Sgamellotti, J. Electron Spectrosc. Relat. Phenom. **76**, 47 (1995).
[16] V. Averbukh and L. S. Cederbaum, J. Chem. Phys. **123**, 204107 (2005).
[17] M. Ohno and G. Wendin, Solid State Commun. **39**, 875 (1981).
[18] C. Verdozzi, M. Cini, J. A. Evans, R. J. Cole, A. D. Laine, P. S. Fowles, L. Duó, and P. Weightman, Europhys. Lett. **16**, 743 (1991).
[19] D. Minelli, F. Tarantelli, A. Sgamellotti, and L. S. Cederbaum, J. Electron Spectrosc. Relat. Phenom. **74**, 1 (1995).
[20] F. Tarantelli, A. Sgamellotti, and L. S. Cederbaum, Phys. Rev. Lett. **72**, 428 (1994).
[21] M. Ohno, J. Electron Spectrosc. Relat. Phenom. **143**, 13 (2005).
[22] C. Verdozzi and M. Cini, Phys. Rev. B **51**, 7412 (1995).
[23] J. J. Lander, Phys. Rev. **91**, 1382 (1953).
[24] M. Cini, Solid State Commun. **20**, 605 (1976).
[25] G. A. Sawatzky, Phys. Rev. Lett. **39**, 504 (1977).
[26] T. Aberg and G. Howat, *Theory of the Auger Effect* (Springer-Verlag, Berlin, 1982).
[27] R. Colle and S. Simonucci, Phys. Rev. A **39**, 6247 (1989).
[28] R. Colle and S. Simonucci, Phys. Rev. A **48**, 392 (1993).
[29] R. Colle, D. Embriaco, M. Massini, S. Simonucci, and S. Taioli, Nucl. Instrum. Methods Phys. Res. B **213**, 65 (2004).
[30] R. Colle, D. Embriaco, M. Massini, S. Simonucci, and S. Taioli, Phys. Rev. A **70**, 042708 (2004).
[31] R. Colle, D. Embriaco, M. Massini, S. Simonucci, and S. Taioli, J. Phys. B **37**, 1237 (2004).
[32] U. Fano, Phys. Rev. **124**, 1866 (1961).
[33] M. A. Spackman and A. S. Mitchell, Phys. Chem. Chem. Phys. **3**, 1518 (2001).
[34] A. Szabo and N. S. Ostlund, *Modern Quantum Chemistry* (Dover, New York, 1996).
[35] J. C. Phillips and L. Kleimann, Phys. Rev. **116**, 287 (1959).
[36] R. Colle and S. Simonucci, Phys. Rev. A **42**, 3913 (1990).
[37] K. L. Yip and W. B. Fowler, Phys. Rev. B **10**, 1400 (1974).
[38] M. P. Seah, I. S. Gilmore, and S. J. Spencer, Appl. Surf. Sci. **144-145**, 178 (1999).
[39] M. P. Seah, J. Electron Spectrosc. Relat. Phenom. **71**, 191 (1995).
[40] M. Cini, Phys. Rev. B **17**, 2486 (1978).
[41] M. V. Zakhvatova, F. Z. Gil'mutdinov, and D. V. Surnin, Phys. Met. Metallogr. **104**, 157 (2007).
[42] R. Shimizu and Z. J. Ding, Rep. Prog. Phys. **55**, 487 (1992).
[43] M. Dapor, *Electron-Beam Interactions with Solids: Applications of the Monte Carlo Method to Electron Scattering Problems*, Springer Tracts in Modern Physics Vol. 186 (Springer, Berlin, 2003).
[44] M. Dapor, Surf. Sci. **600**, 4728 (2006).
[45] M. Filippi, L. Calliari, and M. Dapor, Phys. Rev. B **75**, 125406 (2007).
[46] M. Dapor, J. Appl. Phys. **79**, 8406 (1996).
[47] A. Jablonski, F. Salvat, and C. J. Powell, J. Phys. Chem. Ref. Data **33**, 409 (2004).
[48] R. H. Ritchie, Phys. Rev. **106**, 874 (1957).
[49] U. Buechner, J. Phys. C **8**, 2781 (1975).
[50] J. C. Ashley, J. Electron Spectrosc. Relat. Phenom. **46**, 199 (1988).